

## Bell States of Atoms with Ultralong Lifetimes and Their Tomographic State Analysis

C. F. Roos, G. P. T. Lancaster, M. Riebe, H. Häffner, W. Hänsel, S. Gulde, C. Becher, J. Eschner,  
F. Schmidt-Kaler, and R. Blatt

*Institut für Experimentalphysik, Universität Innsbruck, Technikerstrasse 25, A-6020 Innsbruck, Austria*

(Received 28 July 2003; published 3 June 2004)

Arbitrary atomic Bell states with two trapped ions are generated in a deterministic and preprogrammed way. The resulting entanglement is quantitatively analyzed using various measures of entanglement. For this, we reconstruct the density matrix using single qubit rotations and subsequent measurements with near-unity detection efficiency. This procedure represents the basic building block for future process tomography of quantum computations. As a first application, the temporal decay of entanglement is investigated in detail. We observe ultralong lifetimes for the Bell states  $\Psi_{\pm}$ , close to the fundamental limit set by the spontaneous emission from the metastable upper qubit level and longer than all reported values by 3 orders of magnitude.

DOI: 10.1103/PhysRevLett.92.220402

PACS numbers: 03.65.Wj, 03.65.Ud, 03.67.Mn, 32.80.Pj

In an ion trap quantum computer, qubits are encoded in internal ground or metastable states of confined atoms. Quantum computations [1] are carried out by sequences of single qubit and two-qubit operations which involve entanglement operations in order to realize, for example, the two-qubit controlled-NOT (CNOT) gate operation [2]. The coupling of the qubits to the environment needs to be well understood so that its effect can be minimized. Thus, it is a very important task to investigate the performance of these entanglement operations and to provide a basic tool for future process tomography of more complicated quantum computations. In this Letter, we report on the programmed generation of arbitrary Bell states of two atomic ions. The resulting quantum states are analyzed by reconstructing the corresponding density matrix of the two-atom quantum system. This is achieved by single qubit rotations and subsequent projective measurements. The entanglement is analyzed using various measures. With this technique at hand, we investigate the temporal dynamics of the generated entangled states and demonstrate that certain Bell states survive even in the presence of otherwise decohering field fluctuations. This technique presents a fundamental building block for the state analysis of an ion trap quantum computer and its dynamic evaluation by process tomography.

Quantum state tomography [3] allows the estimation of an unknown quantum state that is available in many identical copies. Its principle of operation has been experimentally demonstrated for various physical systems. Multiqubit states have been investigated in nuclear magnetic resonance experiments [4] as well as in experiments involving entangled photon pairs [5,6]. Yet, no experiment to date has completely reconstructed the quantum state of entangled material qubits [7,8] and analyzed their dynamic evolution.

In this Letter, we first describe the deterministic creation of all four two-ion Bell states, i.e.,  $\Psi_{\pm} = (|10\rangle \pm$

$|01\rangle)/\sqrt{2}$  and  $\Phi_{\pm} = (|11\rangle \pm |00\rangle)/\sqrt{2}$ , where  $|x_1x_2\rangle$ ,  $x_i \in \{0, 1\}$  represents the combined state of the two qubits.

In our experiments, a qubit is encoded in a superposition of internal states of a calcium ion [9]. We use the  $|S_{1/2}, m = -1/2\rangle \equiv |1\rangle$  ground state and the metastable  $|D_{5/2}, m = -1/2\rangle \equiv |0\rangle$  state (lifetime  $\tau_D \sim 1.17$  s [10]) to represent the qubit states. Two  $^{40}\text{Ca}^+$  ions are loaded into a linear Paul trap having vibrational frequencies of  $(2\pi)1.2$  MHz in the axial and  $(2\pi)5$  MHz in the transverse direction. After Doppler and sideband cooling [9], the ions' breathing mode of axial vibration at  $\omega_b = (2\pi)\sqrt{3} \times 1.2$  MHz is in the ground state  $|0_b\rangle$  (99% occupation). Thereafter, the qubits are initialized in the  $|11\rangle$  state. For quantum state engineering, we employ a narrowband Ti:sapphire laser, which is tightly focused onto either one of the two ions. By exciting the  $S_{1/2}$  to  $D_{5/2}$  quadrupole transition near 729 nm ( $\gamma = 0.16$  Hz), we prepare a single ion in a superposition of the  $|0\rangle$  and  $|1\rangle$  states. If the laser excites the transition on resonance ("carrier transition"), the ion's vibrational state is not affected, whereas if the laser frequency is set to the transition's upper motional sideband ("blue sideband"), the electronic states become entangled with the motional states  $|0_b\rangle$  and  $|1_b\rangle$  of the breathing mode. We use an acousto-optical modulator for switching the exciting laser to either the carrier or sideband transition frequency and for controlling the phase of the light field [11,12]. An electro-optical beam deflector switches the laser beam from one ion, over a distance of 5.3  $\mu\text{m}$ , to the other ion within 15  $\mu\text{s}$ . Directing the beam, which has a width of 2.5  $\mu\text{m}$  (FWHM at the focus), onto one ion, the intensity on the neighboring ion is suppressed by a factor of  $2.5 \times 10^{-3}$ . By a sequence of laser pulses of appropriate length, frequency, and phase, the two ions are prepared in a Bell state as described below. For detection of the internal quantum states, we excite the  $S_{1/2}$  to  $P_{1/2}$  dipole transition near 397 nm and monitor the fluorescence for 15 ms

with an intensified CCD camera separately for each ion. Observation of fluorescence indicates that the ion was projected into the  $S_{1/2} \equiv |1\rangle$  state; no fluorescence reveals the  $D_{5/2} \equiv |0\rangle$  state. By repeating the experimental cycle 200 times, the average populations of all product basis states  $|00\rangle$ ,  $|01\rangle$ ,  $|10\rangle$ , and  $|11\rangle$  are determined.

A Bell state is created by applying laser pulses to ion 1 and 2 on the blue sideband and the carrier. Using the Pauli spin matrices  $\sigma_x, \sigma_y, \sigma_z$  [13] and the operators  $b$  and  $b^\dagger$  that annihilate and create a phonon in the breathing mode, we denote single qubit carrier rotations of qubit  $\alpha$  by

$$R_\alpha(\theta, \phi) = \exp\left[i\frac{\theta}{2}(\sigma_x^{(\alpha)} \cos\phi - \sigma_y^{(\alpha)} \sin\phi)\right] \quad (1)$$

and rotations on the blue sideband of the vibrational breathing mode by

$$R_\alpha^+(\theta, \phi) = \exp\left[i\frac{\theta}{2}(\sigma_x^{(\alpha)} b^\dagger \cos\phi - \sigma_y^{(\alpha)} b \sin\phi)\right]. \quad (2)$$

The Bell state  $\Psi_\pm = (|10\rangle \pm |01\rangle)/\sqrt{2}$  is produced by the pulse sequence  $U_{\Psi_\pm} = R_2^+(\pi, \pm\pi/2)R_2(\pi, \pi/2) \times R_1^+(\pi/2, -\pi/2)$  applied to the  $|11\rangle$  state. The pulse  $R_1^+(\pi/2, -\pi/2)$  entangles the motional and the internal degrees of freedom; the next two pulses  $R_2^+(\pi, \pm\pi/2) \times R_2(\pi, \pi/2)$  map the motional degree of freedom onto the internal state of ion 2. Appending another  $\pi$  pulse,  $U_{\Phi_\pm} = R_2(\pi, 0)U_{\Psi_\pm}$ , produces the state  $\Phi_\pm$  up to a global phase. The pulse sequence takes less than 200  $\mu\text{s}$ .

To account for experimental imperfections, the quantum state is described by a density matrix  $\rho$ . For its experimental determination we expand  $\rho$  into a superposition  $\rho = \sum_i \lambda_i O_i$  of mutually orthogonal Hermitian operators  $O_i$ , which form a basis and obey the equation  $\text{tr}(O_i O_j) = 4\delta_{ij}$  [14]. Then the coefficients  $\lambda_i$  are related to the expectation values of  $O_i$  by  $\lambda_i = \text{tr}(\rho O_i)/4$ . For a two-qubit system, a convenient set of operators is given by the 16 operators  $\sigma_i^{(1)} \otimes \sigma_j^{(2)}$ , ( $i, j = 0, 1, 2, 3$ ), where  $\sigma_i^{(\alpha)}$  runs through the set of Pauli matrices 1,  $\sigma_x, \sigma_y, \sigma_z$ , of qubit  $\alpha$ .

The reconstruction of the density matrix  $\rho$  is accomplished by measuring the expectation values  $\langle \sigma_i^{(1)} \otimes \sigma_j^{(2)} \rangle_\rho$ . A fluorescence measurement projects the quantum state into one of the states  $|x_1 x_2\rangle$ ,  $x_i \in \{0, 1\}$ . By repeatedly preparing and measuring the quantum state, the average population in states  $|x_1 x_2\rangle$  is obtained from which we calculate the expectation values of  $\sigma_z^{(1)}$ ,  $\sigma_z^{(2)}$ , and  $\sigma_z^{(1)} \otimes \sigma_z^{(2)}$ . To measure operators involving  $\sigma_y$ , we apply a transformation  $U$  that maps the eigenvectors of  $\sigma_y$  onto the eigenvectors of  $\sigma_z$ , i.e.,  $U\sigma_y U^{-1} = \sigma_z$ , where  $U = R(\pi/2, \pi)$ . Similarly, the operator  $\sigma_x$  is transformed into  $\sigma_z$  by choosing  $U = R(\pi/2, 3\pi/2)$ . Therefore, all expectation values can be determined by measuring  $\sigma_z^{(1)}$ ,  $\sigma_z^{(2)}$ , or  $\sigma_z^{(1)} \otimes \sigma_z^{(2)}$ . To obtain all 16 expectation values, nine different settings have to be used. For each setting, the experiment is repeated 200 times at a repetition rate of

50 Hz. The whole reconstruction process is therefore completed in less than 40 s. Since a finite number of experiments allows only for an estimation of the expectation values  $\langle \sigma_i^{(1)} \otimes \sigma_j^{(2)} \rangle_\rho$ , the reconstructed matrix  $\rho_R$  is not guaranteed to be positive semidefinite [15]. We avoid this problem by employing a maximum likelihood estimation of the density matrix [15,16], following the procedure as suggested and implemented in Refs. [16–18].

For the pulse sequence that is designed to produce the state  $\Psi_+ = (|10\rangle + |01\rangle)/\sqrt{2}$ , we obtain the density matrix  $\rho_{\Psi_+}$  shown in Fig. 1(a). The fidelity  $F$  of the reconstructed state is  $F = \langle \Psi_+ | \rho_{\Psi_+} | \Psi_+ \rangle = 0.91$ . To produce

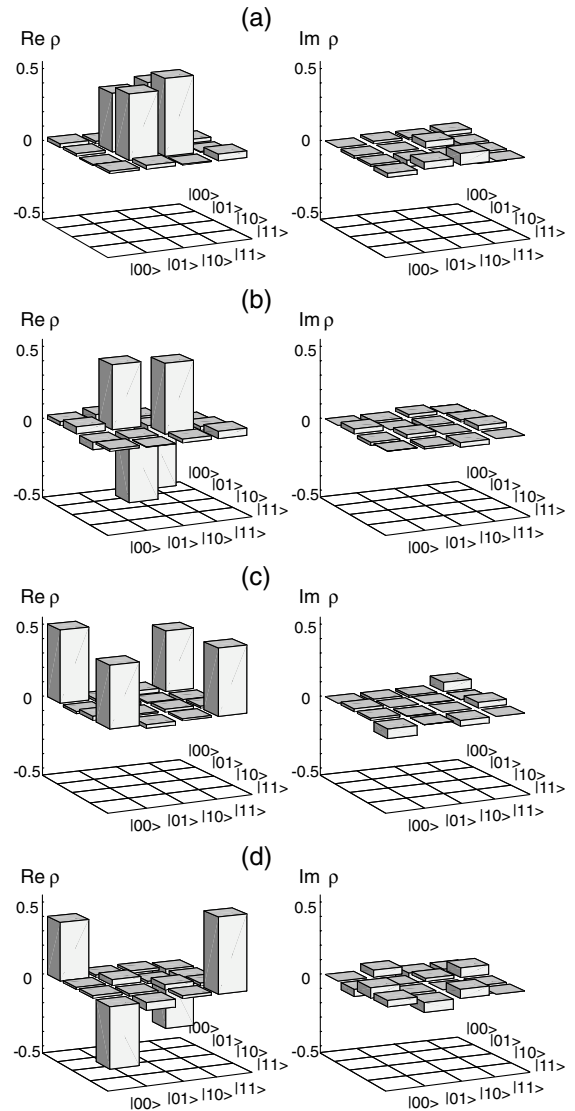


FIG. 1. (a) Real and imaginary parts of the density matrix  $\rho_{\Psi_+}$  that approximates  $\Psi_+ = (|10\rangle + |01\rangle)/\sqrt{2}$ . The measured fidelity is  $F_{\Psi_+} = \langle \Psi_+ | \rho_{\Psi_+} | \Psi_+ \rangle = 0.91$ . (b) Real and imaginary parts of the density matrix  $\rho_{\Psi_-}$  that approximates  $\Psi_- = (|10\rangle - |01\rangle)/\sqrt{2}$ . The measured fidelity is  $F_{\Psi_-} = 0.90$ . (c),(d) Density matrix elements of (c)  $\rho_{\Phi_+}$  and (d)  $\rho_{\Phi_-}$ . Here,  $F_{\Phi_+} = 0.91$  and  $F_{\Phi_-} = 0.88$ .

the state  $\rho_{\Psi_-} = (|10\rangle - |01\rangle)/\sqrt{2}$ , we change the phase of the sideband  $\pi$  pulse by  $\pi$  and experimentally obtain the density matrix  $\rho_{\Psi_-}$  shown in Fig. 1(b). For  $\Phi_{\pm} = (|11\rangle \pm |00\rangle)/\sqrt{2}$ , we find the density matrices depicted in Figs. 1(c) and 1(d).

Having reconstructed a Bell state's density matrix, we can now check that the two qubits are indeed entangled. It has been shown that a mixed state  $\rho$  of two qubits is entangled if and only if its partial transpose  $\rho^{\text{PT}}$  has a negative eigenvalue [19,20]. Not surprisingly, the partial transpose of the density matrix  $\rho_{\Psi_+}$  [Fig. 1(a)] has eigenvalues  $\{-0.42(2), 0.40(2), 0.49(2), 0.53(3)\}$  close to the values of a maximally entangled state  $\{-0.5, 0.5, 0.5, 0.5\}$ . Errors in the determination of the density matrix elements and of quantities derived from them occur mainly as a consequence of quantum projection noise. Systematic effects such as pulse length errors or addressing errors (coherent excitation of an ion by stray light) play a minor role. We estimate the magnitude of quantum projection noise by a bootstrapping technique [21] where the reconstructed density matrix serves for calculating probability distributions used in a Monte Carlo simulation of our experiment.

Among the different measures put forward to quantify the entanglement of mixed bipartite states, the entanglement of formation  $E$  has the virtue of being analytically calculable from the density matrix of a two-qubit system. For a separable state  $E = 0$ , whereas  $E = 1$  for a maximally entangled state. Using the formula given by Wootters [22], we find  $E(\rho_{\Psi_+}) = 0.79(4)$ . For  $\Psi_-$  and  $\Phi_{\pm}$ , we measure  $E(\rho_{\Psi_-}) = 0.75(5)$ ,  $E(\rho_{\Phi_+}) = 0.76(4)$ , and  $E(\rho_{\Phi_-}) = 0.72(5)$ .

All of these Bell states violate a Clauser-Horne-Shimony-Holt inequality. For the state  $\rho_{\Psi_+}$ , for example, we obtain  $\langle A \rangle = 2.52(6) > 2$ , where we have introduced the operator  $A = \sigma_x^{(1)} \otimes \sigma_{x-z}^{(2)} + \sigma_x^{(1)} \otimes \sigma_{x+z}^{(2)} + \sigma_z^{(1)} \otimes \sigma_{x-z}^{(2)} - \sigma_z^{(1)} \otimes \sigma_{x+z}^{(2)}$ , with  $\sigma_{x\pm z} = (\sigma_x \pm \sigma_z)/\sqrt{2}$ .

Once a Bell state has been produced, we monitor its evolution in time by waiting for a time  $t$  before performing a state estimation. We expect the Bell states  $\Psi_{\pm}$  to be immune against collective dephasing due to fluctuations of the magnetic field or the laser frequency [23]. However, they will be time invariant only if the energy separation  $\hbar\omega$  between the qubit states  $|0\rangle$  and  $|1\rangle$  is the same for both qubits. A magnetic field gradient gives rise to slightly different Zeeman shifts on qubits 1 and 2, leading to a linear time evolution of the relative phase between the  $|01\rangle$  and the  $|10\rangle$  component of the  $\Psi_{\pm}$  states. This is observed in our experiments. We calculate the maximum overlap  $F_m = \max_{\beta} (\langle \Psi_{\beta} | \rho_{\Psi_+}(\tau) | \Psi_{\beta} \rangle)$  between the density matrix  $\rho_{\Psi_+}(\tau)$  and the states  $\Psi_{\beta} = 1/\sqrt{2}(|10\rangle + \exp(i\beta)|01\rangle)$  as a function of time. Figure 2(a) shows the phase  $\beta_m(\tau)$  for which the maximum overlap  $F_m$  is obtained.

The phase changes linearly with time according to  $\beta_L = \omega_{\beta}\tau$  with  $\omega_{\beta} = (2\pi)170$  Hz, revealing a field gra-

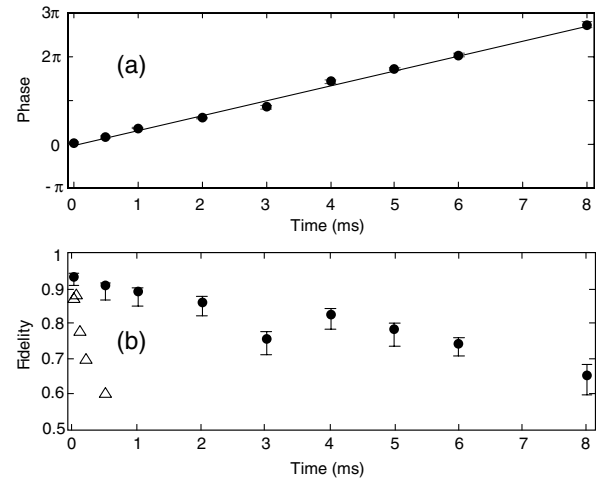


FIG. 2. Time evolution of the state  $\Psi_+ = (|10\rangle + |01\rangle)/\sqrt{2}$ . A magnetic field gradient causes the relative phase between the  $|10\rangle$  and the  $|01\rangle$  parts to evolve linearly in time. Decoherence leads to a loss of fidelity. (a) Phase  $\beta_m(t)$  for which the overlap  $F_m = \max_{\beta} (\langle \Psi_{\beta} | \rho_{\Psi_+}(\tau) | \Psi_{\beta} \rangle)$  between  $\rho_{\Psi_+}(\tau)$  and states of type  $\Psi_{\beta} = (|10\rangle + \exp(i\beta)|01\rangle)/\sqrt{2}$  is maximized. (b) Fidelity  $F = \langle \Psi_{\beta_L}(\tau) | \rho(\tau) | \Psi_{\beta_L}(\tau) \rangle$  of the measured density matrix  $\rho(\tau)$  that nominally corresponds to the state  $\Psi_{\beta_L}(\tau) = (|10\rangle + \exp(i\beta_L)|01\rangle)/\sqrt{2}$  (solid circles). The state  $\Phi_+ = (|11\rangle + |00\rangle)/\sqrt{2}$  (triangles) is sensitive to fluctuations of the laser frequency and the magnetic field. Thus, its decay occurs on a much shorter time scale. Error bars account for quantum projection noise as well as systematic errors in the reconstruction process. They are derived from a Monte Carlo simulation.

dient of  $dB/dz = 0.6$  G/cm in the direction of the ion string that leads to a fully deterministic transformation from a  $\Psi_+$  state into a  $\Psi_-$  state every 3 ms and vice versa [24]. The decay of the Bell state into a mixed state leads to a slow decline of the fidelity  $F = \langle \Psi_{\beta_L} | \rho_{\Psi_+}(\tau) | \Psi_{\beta_L} \rangle$

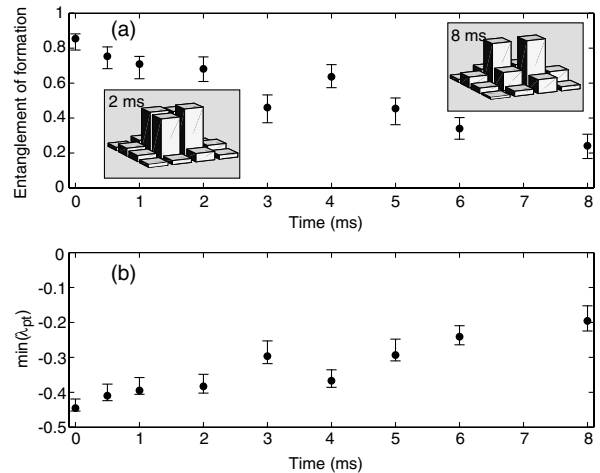


FIG. 3. Decay of the Bell state into a statistical mixture as a function of time. (a) Entanglement of formation and (b) smallest eigenvalue of the partial transpose of the density matrix. The insets show the magnitude of the density matrix elements measured after a time of 2 ms and 8 ms.

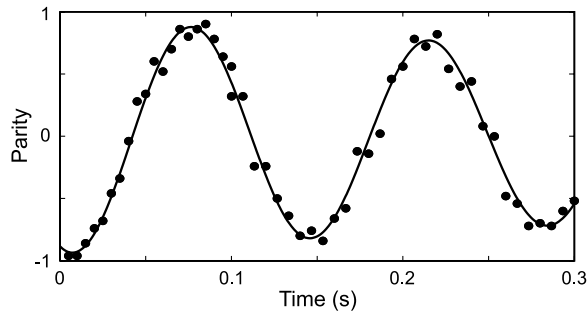


FIG. 4. Time evolution of the expectation value  $\langle \sigma_x^{(1)} \otimes \sigma_x^{(2)} \rangle$  for state  $\rho_\Psi(t)$ . The oscillation at  $f = 7.2(1)$  Hz is caused by the residual magnetic field gradient; the damping stems predominantly from spontaneous emission from the metastable upper qubit level  $D_{5/2}$ .

over time, which is shown in Fig. 2(b). The  $\Psi_\pm$  states decay with a decoherence time of 5 ms into a statistical mixture, whereas the  $\Phi_\pm$  states already decay after about 200  $\mu$ s to a fidelity of  $F = 0.75$ . This decay can also be seen by tracing the entanglement of formation or the smallest eigenvalue of the partial transpose as a function of time as shown in Fig. 3.

We identified the loss of coherence to be predominantly caused by spatially inhomogeneous, time-varying ac-Stark shifts induced by a nonresonant repumping laser at 866 nm. After installing fast shutters and improving the homogeneity of the magnetic field, the entanglement persisted for several 100 ms. In Fig. 4, we produce the state  $\Psi_-$  and measure the expectation value  $\langle \sigma_x^{(1)} \otimes \sigma_x^{(2)} \rangle$  as a function of time. As in Fig. 2, the magnetic field gradient gives rise to a sinusoidal variation of the signal with time. Decay of the metastable  $D_{5/2}$  level would result in an exponential decay with a decay time of  $\tau = 1.17$  s. We find  $\tau = 1.05(0.15)$  s and infer that spontaneous emission indeed limits the persistence of our entangled states. Note that the entanglement lifetime exceeds previously published results by 3 orders of magnitude [23] which lends support to the idea of using entangled states for atomic clocks based on trapped ions [25].

With the methods demonstrated above, we have deterministically created all four Bell states and obtained complete information about the two-qubit quantum states. We expect that this will be an important tool for manipulating and analyzing more complex multiqubit systems and quantum gate operations applied to them.

C. R. acknowledges useful discussions with Z. Hradil. H. H. is funded by the Marie-Curie-program of the European Union. We gratefully acknowledge support by the European Commission [QUEST (No. HPRN-CT-

2000-00121) and QGATES (No. IST-2001-38875) networks], by the ARO (No. DAAD19-03-1-0176), by the Austrian Science Fund (FWF), and by the Institut für Quanteninformation GmbH.

- 
- [1] M. A. Nielsen and I. L. Chuang, *Quantum Computation and Quantum Information* (Cambridge University, Cambridge, 2000).
  - [2] F. Schmidt-Kaler *et al.*, Nature (London) **422**, 408 (2003); D. Leibfried *et al.*, *ibid.* **422**, 412 (2003).
  - [3] K. Vogel and H. Risken, Phys. Rev. A **40**, 2847 (1989).
  - [4] I. L. Chuang, N. Gershenfeld, M. G. Kubinec, and D. Leung, Proc. R. Soc. London, Ser. A **454**, 447 (1998).
  - [5] A. G. White, D. F. V. James, P. H. Eberhard, and P. G. Kwiat, Phys. Rev. Lett. **83**, 3103 (1999).
  - [6] A. G. White, D. F. V. James, W. J. Munro, and P. G. Kwiat, Phys. Rev. A **65**, 012301 (2001).
  - [7] E. Hagle, X. Maître, G. Nogues, C. Wunderlich, M. Brune, J. M. Raimond, and S. Haroche, Phys. Rev. Lett. **79**, 1 (1997).
  - [8] Q. A. Turchette, C. S. Wood, B. E. King, C. J. Myatt, D. Leibfried, W. M. Itano, C. Monroe, and D. J. Wineland, Phys. Rev. Lett. **81**, 3631 (1998).
  - [9] Ch. Roos *et al.*, Phys. Rev. Lett. **83**, 4713 (1999).
  - [10] P. A. Barton, C. J. S. Donald, D. M. Lucas, D. A. Stevens, A. M. Steane, and D. N. Stacey, Phys. Rev. A **62**, 032503 (2000).
  - [11] F. Schmidt-Kaler *et al.*, Appl. Phys. B **77**, 789 (2003).
  - [12] H. Häffner *et al.*, Phys. Rev. Lett. **90**, 143602 (2003).
  - [13] Note that  $|0\rangle$  and  $|1\rangle$  are eigenvectors of  $\sigma_z$  corresponding to the eigenvalues  $+1$  and  $-1$ , respectively.
  - [14] U. Fano, Rev. Mod. Phys. **29**, 74 (1957).
  - [15] Z. Hradil, Phys. Rev. A **55**, R1561 (1997).
  - [16] K. Banaszek, G. M. D'Ariano, M. G. A. Paris, and M. F. Sacchi, Phys. Rev. A **61**, 010304 (1999).
  - [17] D. F. V. James, P. G. Kwiat, W. J. Munro, and A. G. White, Phys. Rev. A **64**, 052312 (2001).
  - [18] K. Usami, Y. Nambu, Y. Tsuda, K. Matsumoto, and K. Nakamura, Phys. Rev. A **68**, 022314 (2003).
  - [19] A. Peres, Phys. Rev. Lett. **77**, 1413 (1996).
  - [20] M. Horodecki, P. Horodecki, and R. Horodecki, Phys. Lett. A **223**, 1 (1996).
  - [21] B. Efron and R. Tibshirani, Stat. Sci. **1**, 54 (1986)
  - [22] W. K. Wootters, Phys. Rev. Lett. **80**, 2245 (1998).
  - [23] D. Kielpinski, V. Meyer, M. A. Rowe, C. A. Sackett, W. M. Itano, C. Monroe, and D. J. Wineland, Science **291**, 1013 (2001).
  - [24] The value of the field gradient was confirmed in an independent measurement.
  - [25] J. J. Bollinger, W. M. Itano, D. J. Wineland, and D. J. Heinzen, Phys. Rev. A **54**, R4649 (1996).